Nanoscale Advances

REVIEW

View Article Online
View Journal | View Issue

Cite this: *Nanoscale Adv.*, 2022, **4**, 4197

N-doped graphene for electrocatalytic O_2 and CO_2 reduction

Ruguang Ma, [a] Kuikui Wang, [b] Chunjie Li,[a] Chundong Wang, [c] Aziz Habibi-Yangjeh*[d] and Guangcun Shan*[e]

The electrocatalytic CO_2 reduction reaction (CO_2RR) and oxygen reduction reaction (ORR) are important approaches to realize energy conversion and sustainable development. However, sluggish reaction kinetics severely hinders the practical application of devices related to these reactions. N-doped graphene (NG) with unique properties exhibits great potential in catalyzing the CO_2RR and ORR, which is attributed to the electron redistribution. In this review, we start from the fundamental properties of NG, especially emphasizing the changes caused by N doping. Then the synthetic methods are summarized by classifying them into top-down strategies and bottom-up strategies. Subsequently, the applications of NG in the ORR and CO_2RR are discussed and the effects of electronic structure on the electrocatalytic activity are highlighted. Finally, we give our own perspective on the future research direction of NG in the applications of the ORR and CO_2RR.

Received 2nd June 2022
Accepted 29th August 2022

DOI: 10.1039/d2na00348a

rsc.li/nanoscale-advances

1. Introduction

To mitigate the global climate problem and achieve carbon neutrality, the conversion and storage of renewable energy highly demand advanced electrochemical technologies, most of which involve various electrocatalytic reactions. For instance, the oxygen reduction reaction (ORR) is a critical electrochemical process in metal-air batteries and fuel cells.[1–4] The electrocatalytic CO_2 reduction reaction (CO_2RR) is especially an effective strategy to re-balance the carbon cycle and to harvest value-added chemical products.[5–7] However, these electrocatalytic processes have been severely limited by the sluggish reaction kinetics, which necessitate efficient electrocatalysts with good selectivity and durability. Although the state-of-art noble metal-based electrocatalysts have been used in these reactions,[8,9] the scarcity accompanied by high cost hampers the large-scale applications of these sustainable energy technologies. It is highly desirable to discover and design cost-effective electrocatalysts.

Among many non-precious-metal materials, graphene consisting of sp^2-hybridized carbon atoms arranged in a honeycomb lattice has been intensively studied as a potential candidate,[10] due to the outstanding electronic conductivity, large specific surface area, and good mechanical properties arising from the unique two-dimensional (2D) structure.[11,12] As a spark, it also inspires the exploration of other 2D materials and broadens the 2D material family, including transition dichalcogenides (TMDs), MXenes, hexagonal boron nitride (h-BN), *etc.*[13–16] Graphene can be built into different nanostructures, such as graphene quantum dots,[17] graphene nanoribbons,[18] and graphene nanomeshes[19] as well as recently emerged "magic-angle graphene",[20] demonstrating various novel properties,[21] which attract the intensive interest of researchers around the world. Moreover, heteroatom doping into graphene also plays an important role in the modulation of fundamental properties.[22] Among various heteroatoms, the doping of nitrogen (N) atoms usually leads to strong charge polarization in the carbon plane due to the remarkable difference of electronegativity between nitrogen (χ = 3.04 on the Pauling scale) and carbon (χ = 2.55).[23]

Since the pioneering work of N-doped carbon nanotubes used for the electrocatalytic ORR,[24] N-doped carbon materials gained special attention for electrocatalysis applications.[25] In particular, N-doped graphene (NG) has been placed at the center of the spotlight, due to the unique characteristics and advantages of the structure and properties, including the induced charge redistribution and defects by N doping.[26] Moreover, NG has been extensively explored as an electrocatalyst for the CO_2RR to play an ever-increasingly important role in realizing carbon neutrality and ecosystem protection.[27–29]

[a]*School of Materials Science and Engineering, Suzhou University of Science and Technology, 99 Xuefu Road, Suzhou, 215011, China*

[b]*Institute of Materials for Energy and Environment, Laboratory of New Fiber Materials and Modern Textile, Growing Basis for State Key Laboratory, College of Materials Science and Engineering, Qingdao University, Qingdao 266071, China*

[c]*School of Optical and Electronic Information, Wuhan National Laboratory for Optoelectronics, Optics Valley Laboratory, Huazhong University of Science and Technology, Wuhan 430074, PR China*

[d]*Department of Chemistry, Faculty of Science, University of Mohaghegh Ardabili, Ardabil, Iran. E-mail: ahabibi@uma.ac.ir*

[e]*School of Instrumentation Science and Opto-electronics Engineering, Beihang University, No. 37 XueYuan Road, Beijing 100083, China. E-mail: gcshan@buaa.edu.cn*

Therefore, it is of significance to review the recent advances of NG applications in these reactions and to figure out the opportunities and challenges in the future.

In this review, we primarily start from the fundamental properties of NG followed by the synthesis methods. Then, we summarize the applications of NG in the ORR and CO_2RR and emphasize the effects of the electronic structure on the electrocatalytic activity. Based on the specific reaction pathway, we try to construct the correlation between the physicochemical properties and electrocatalytic activity and to elucidate the electrocatalytic reaction mechanism. Finally, we will provide an outlook on the future research direction and give our own perspective on NG in the applications of the ORR and CO_2RR.

2. Fundamental properties

Graphene is an sp^2-hybridized carbon layer with zero bandgap. Heteroatom doping into graphene, especially N doping, can effectively tailor its electronic structure and other intrinsic properties, broadening the application fields.[30] There are usually several N species in N-doped graphene (NG), including graphitic N, pyridinic N, pyrrolic N, amide N and N oxides as shown in Fig. 1a. The successful doping of N atoms into the graphene lattice can be revealed by the scanning tunneling microscopy (STM) image (Fig. 1b) and simulated STM image computed from the local density of states for graphitic doping (Fig. 1c).[31] The introduction of an N dopant at different locations leads to different electronic states. For example, the formation of the lone pair at pyridinic N makes the N atom negatively charged (Fig. 1d).[32] And the spatial propagation of the localized π states can be seen in the STM simulations at a negative bias of -1.0 V, as shown in Fig. 1e and f.[32] The charge transfer caused by N doping induces net positive charge at adjacent C atoms, which facilitates the attraction of electrons from the anode and the ORR.[33] The charge redistribution also changes the chemisorption mode of the O_2 molecule from the usual end-on adsorption (Pauling model) to side-on adsorption (Yeager model),[24] which could effectively weaken the O–O bonding in parallel diatomic adsorption. With the development of synthetic methods and advanced characterization techniques, the understanding on the fundamental properties of NG has been deepened gradually.

The band structure and density of states (DOS) calculated by the *ab initio* method and tight-binding (TB) model indicate an obvious bandgap opening, as shown in Fig. 2a & b.[34] When different concentrations of N dopants are randomly distributed in one sublattice, the bandgap (E_g) ranges from 45, 110, 340 to 550 meV for various N concentrations corresponding to 0.5, 1, 4, and 8 at% (Fig. 2b).[34] Experimentally, compared to that of pristine graphene, the Raman spectrum of NG shows an obvious D′-band, which is attributed to the intravalley double resonance scattering processes (Fig. 2c).[35] And a more intense D-band is also shown, which probably originates from the elastically scattered photo-excited electron created by the large number of N atoms embedded in the graphene lattice before emitting a phonon. There is also an obvious downshift

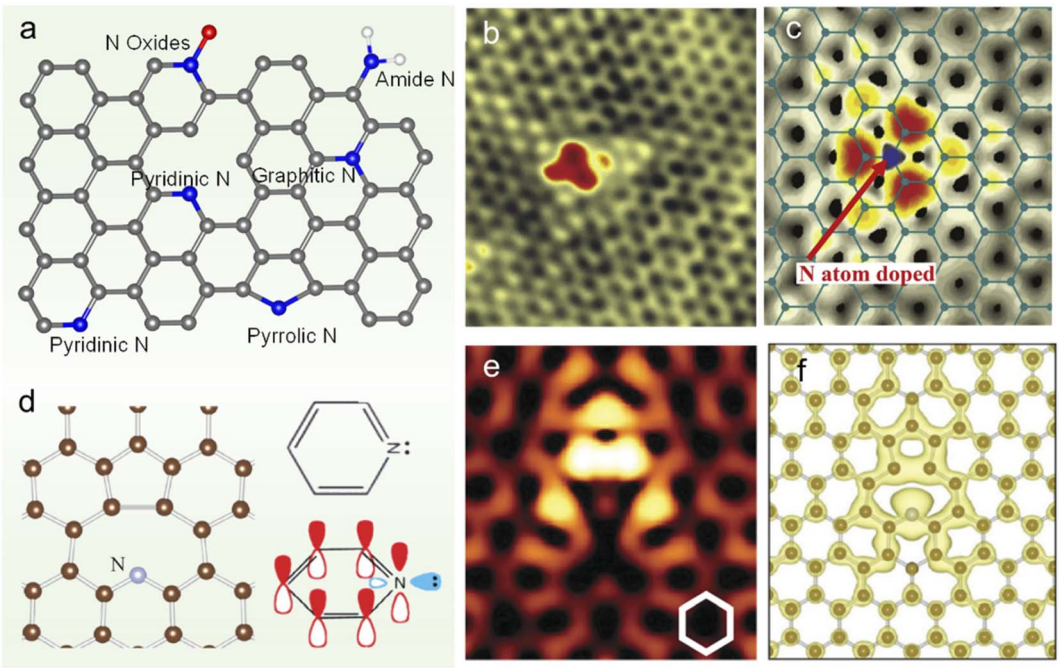

Fig. 1 (a) Scheme of NG with different N species, (b) STM image of monolayer NG and (c) its simulation by DFT calculations. (d) Equilibrium geometry of pyridinic N calculated by DFT (left panel) and schematic representation of p_z orbitals in pyridinic N (right panel). (e) Simulated STM images (constant-current mode) for pyridinic N graphene at a bias voltage of -1.0 V. The N atom is placed at the center of the image. (f) DFT equilibrium geometry and isosurface plot of electron density at 1.5×10^{-3} electrons/Å^3 integrated from the Fermi level to -0.7 eV. (b and c) Reprinted with permission from ref. 31, copyright © 2011 AAAS. (d–f) Reprinted from ref. 29 with permission from ref. 32, copyright © American Physical Society 2012.

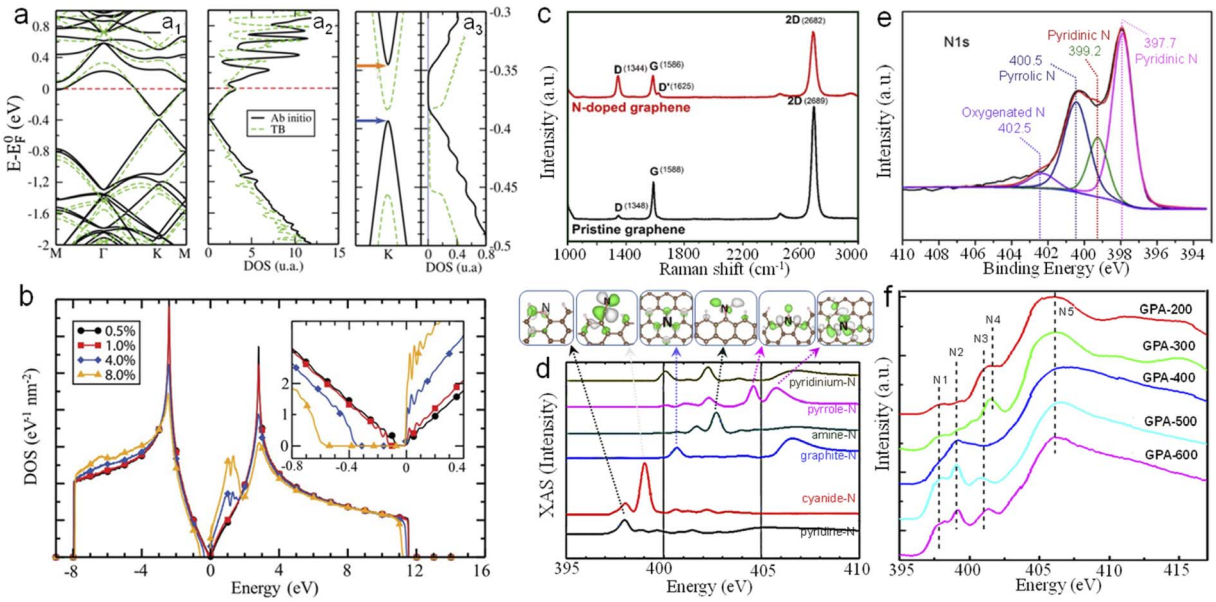

Fig. 2 (a) *Ab initio* and tight-binding (a_1) band structures and (a_2) density of states (DOS) of a 10 × 10 graphene supercell containing one substitutional N dopant. (a_3) Zoomed view of the band structure (left panel) and DOS (right panel) close to the band gap. (b) DOS of graphene containing various concentrations of N dopants randomly distributed in one sublattice; inset: zoomed view of the DOS in the band gap region. (c) Raman spectrum of NG and pristine graphene. (d) Theoretically calculated XAS of NG. (e) High resolution N1s XPS spectra of NG obtained by annealing glucose and melamine at 550 °C firstly and then at 800 °C. (f) N K-edge XANES spectra of NG prepared by annealing a GO/urea mixture at different temperatures (200, 300, 400, 500 and 600 °C). (a and b) Reprinted with permission from ref. 34, copyright © American Chemical Society 2013. (d) Reprinted with permission from ref. 38, copyright © American Chemical Society American Physical Society 2011. (f) Reprinted with permission from ref. 40, copyright© Elsevier Ltd 2011.

of the G-band and 2D band caused by the movement of the Fermi level.

Different N configurations in NG have different influences on the electrocatalytic performance. Theoretical studies reveal that the doped N located at the zigzag edge of graphene can activate the neighboring edge carbons toward the ORR, while for a given zigzag edge, the presence of pyridinic N significantly reduces the inherent ORR activity of graphene.[36,37] Moreover, Wang *et al.* studied the nitrogen configuration and its location (armchair or zigzag edge) in NG by using theoretical calculations and presented the K-edge X-ray absorption spectra (XAS) and emission spectra (XES) as well as the final (initial)-state wave functions (Fig. 2d).[38] Experimentally, the characteristic peaks can be measured and deconvoluted by X-ray photoelectron spectroscopy (XPS) and X-ray absorption near-edge structure spectroscopy (XANES) as shown in Fig. 2e and f. The high-resolution XPS spectrum of N1s can be fitted into four peaks at around 397.7, 399.2, 400.5 and 402.5 eV, which are assigned to pyridinic N, pyrrolic N, graphitic N and oxygenated N, respectively (Fig. 2e).[39] As shown in Fig. 2f, the N K-edge XANES spectrum of NG changes with the annealing temperature from 200 to 600 °C, indicating the corresponding variation of N species.[40] Especially, the N5 peak at ~406 eV in GPA-200 is ascribed to the σ* excitation of C–N bonds, while N_4 at ~402 eV can be attributed to the attachment of urea species. Moreover, amino induced small features at about 399 eV (N_1 and N_2) can also be observed. With the increase of temperature, the N_4 peak gradually decreases and a strong N_2 peak emerges. When the temperature reaches 500 °C, the N_1 peak and N_3 peak ascribed to the pyridinic type and graphitic type, respectively, are observed. And the graphitic N species become dominant with the N_3 peak increasing greatly at 600 °C. These results provide significant guidance for the identification of N species in NG experimentally synthesized by different methods.

3. Synthetic methods

Generally, the synthesis of graphene can be classified into two main strategies: top-down and bottom-up methods.[41,42] Top-down strategies refer to cutting or tearing graphite into graphene, including mechanical exfoliation, chemical ablation, electrochemical oxidation, plasma treatment, *etc.* Bottom-up methods realize the synthesis of graphene from molecular precursors containing a certain number of conjugated carbon atoms or from the gas-phase vapor growth. To realize the substitution or doping of N atoms into the graphene lattice, several treatment methods are usually employed.

3.1 Top-down strategies

3.1.1 Thermal annealing. Thermal annealing is a simple method to prepare NG by heat-treating a mixture of graphene/graphene oxide and N-containing sources. For example, Dai's group developed N-doped reduced graphene oxide (rGO) *via* thermal annealing of GO in an NH_3 atmosphere, which can occur at a temperature as low as 300 °C.[43] They also found that the doping process is accompanied by the reduction of GO,

where the oxygen level decreases from ~28% in GO down to ~2% upon thermal annealing with NH_3 gas at 1100 °C. Oxygen groups in GO were found to be responsible for reactions with NH_3 and C–N bond formation. The sample with the highest N-doping level was annealed at 500 °C and the N level decreases with the increase of temperature. Besides NH_3 gas, other N-containing sources were utilized to react with GO to form NG at an elevated temperature, such as urea, polypyrrole, and melamine. The N content in NG can reach as high as about 15 at%.[44]

3.1.2 Hydrothermal method. Different from thermal annealing, the hydrothermal method is another facile way to obtain NG by heat-treating a mixture of GO and N-containing precursors in solution at different temperatures.[45] N-containing precursors include polypyrrole, $NH_4 \cdot H_2O$, $N_2H_4 \cdot H_2O$, urea, *etc.* In a typical process, GO dispersed in solution is mixed with a certain amount of N-containing precursor, such as urea, under sonication. Afterwards the solution was sealed in a teflon-lined autoclave and maintained at an elevated temperature, *e.g.*, 180 °C for hours. After cooling to room temperature, the final product is washed with distilled water and ethanol, and dried at about 60 °C.

3.1.3 Microwave method. Microwave reduction is a rapid method to reduce GO to pristine graphene *via* one- to two-second pulses of microwaves,[46,47] because GO can absorb microwaves easily and reach a very high temperature (500 °C) in a few seconds. Pure graphene is a dielectric material with an sp2 bonded carbon network, which contains abundant delocalized π electrons. In an external electric field, these electrons start moving in the direction of the field and generate an electric current. As these charge carriers cannot keep up with the change of the phase in an alternating field, the produced energy is dissipated in the form of heat.[48,49] Both GO and rGO are polar materials due to the presence of oxygen functional groups. In the presence of an electromagnetic field, the alternating electric field forces the dipoles to align themselves in phase with the field, thus generating stretching and bending vibrations, which subsequently are dissipated in the form of heat energy.[50] During the microwave-reduction process, N doping can be achieved in an NH_3 atmosphere. Typically, graphite oxide is placed in a three-neck flask purged with NH_3 at a certain rate for several minutes through a mass flow controller. Then the flask was placed in a microwave oven under high power for tens of seconds with the flow of NH_3 in the whole process. Finally, NG can be obtained through the microwave-thermal expansion procedure.[51] In addition, microwave-assisted hydrothermal heating is a combined method to obtain NG by mixing the GO and N sources in a microwave reactor.[52]

3.1.4 Plasma treatment. Plasma treatment is an effective approach to modify the material surface, which can be used for the incorporation of heteroatoms in graphene. Plasma is a gas of charged particles, which can be generated by heating a gas or by applying strong electromagnetic fields.[53] These charged particles make the plasma electrically conductive. The N_2^+ ions from N_2 plasma initiated by a high bias voltage are able to generate defects and create covalent bonds with pre-existing defect sites.[54] For the typical synthesis of NG, graphene is firmly attached onto a glassy carbon electrode (GCE) and then was placed in a plasma chamber, which was backfilled with a nitrogen atmosphere at a specific pressure. The plasma power and treatment time can be tailored for a targeted composition or structure.[55] By using synchrotron-based scanning photoemission microscopy (SPEM), Choi and coworkers found that N doping takes place not only at the active edges but also at the basal plane (Fig. 3a).[56] Moreover, with the increase of treatment duration, at basal planes the pyrrole-N portion increases but the graphite-N portion decreases, and the pyrrole-N portion appears

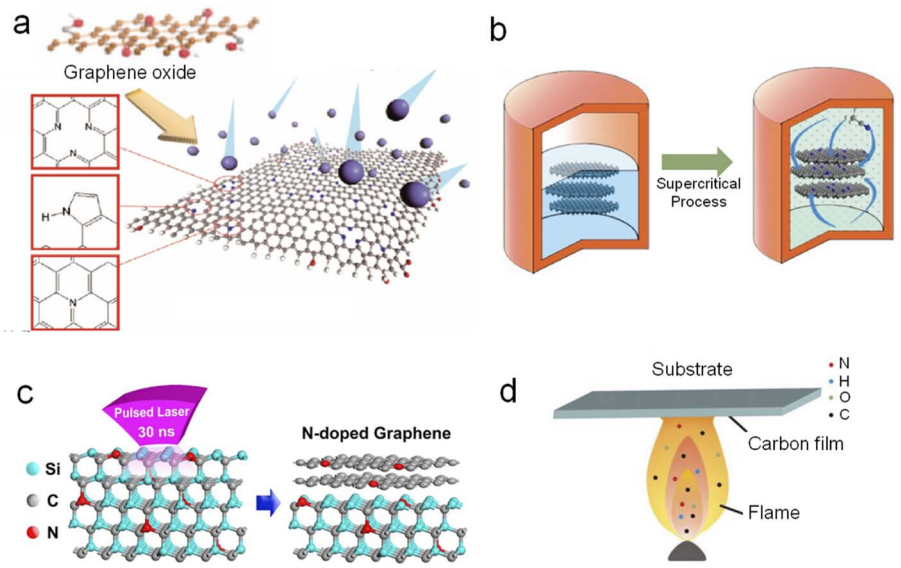

Fig. 3 Synthetic methods of NG: (a) plasma treatment, (b) supercritical reaction, (c) pulsed laser irradiation, and (d) flame treatment. (a), (b) and (c) Reprinted with permission from ref. 56, 60, and 61, copyright© 2011 and 2014 American Chemical Society. (d) Reprinted from ref. 62, copyright© 2012 Elsevier B.V.

higher at edges than at basal planes. N configuration in graphene is highly affected by the vacancy defect species in graphene, because the plasma can stimulate various vacancies, such as divacancies and monovacancies.[57] Moreover, the thermal spike caused by prolonging implantation time or increasing implantation energy can lead to the conversion from pyrrolic-N to pyridinic-N.

3.1.5 Arc-discharge method. Arc discharge between two graphite electrodes under a relatively high pressure of hydrogen can yield graphene flakes in a water-cooled stainless steel chamber.[58] When NH_3 is used as one of the buffer gases, the generated graphene sheets are doped by N atoms on a large scale, which could be applied to successive production. In a typical process, two electrodes were both pure graphite rods with a diameter of 8 mm, and the current was held at 120 A.[59] As the rods were brought close enough, discharge occurred and plasma formed. The anode was vaporized in a He and NH_3 mixed atmosphere of 760 Torr. To keep a constant distance of 1 mm between the two electrodes, the cathode was kept rotating with the reduction of the anode.

There are also other methods used for synthesizing NG, which are not so popular as the abovementioned methods, for example, supercritical reaction (Figure 3b),[60] pulsed laser irradiation (Fig. 3c),[61] and flame treatment (Fig. 3d).[62] The supercritical reaction is readily employed to prepare NG at a relatively low temperature of about 310 °C. In a typical procedure, few-layer graphene sheets (2 mg) were dispersed in acetonitrile (25 mL), and the mixture was transferred to a corundum-lined autoclave (50 mL).[60] The autoclave was heated to 310 °C and an environment of supercritical reaction fluid was maintained within the autoclave. After a certain reaction time, N-doped graphene sheets can be harvested after centrifugation and rinsing. Laser irradiation can also provide enough heat for direct *in situ* growth of NG on an insulating substrate and does not need a complicated transfer process. By virtue of flame treatment, Pan's group prepared NG with dominant pyridine-N from amine plus ethanol flames.[62] During the process, a Si substrate with a Ni film was inserted into the flame at 5.5 cm above a lamp for 1 min. A brown combustion product, *i.e.*, NG, was observed on the substrate when it was withdrawn from the flame.

3.2 Bottom-up strategies

3.2.1 Chemical vapor deposition (CVD). The CVD method is a popular approach to obtain large-area and high-quality graphene and heteroatom-doped graphene. For the synthesis of NG, the C and N precursors are introduced onto the surface of a hot substrate (*e.g.*, Cu or Ni) to realize the formation of C–C and C–N bond networks at a high temperature (>800 °C).[63,64] In the synthesis process, Cu or Ni not only serves as the substrate, but also functions as a catalyst to tune the growth of graphene. To lower the temperature, plasma-enhanced CVD (PECVD) and thermal CVD were also employed to grow NG (Fig. 4a).[65,66] During the CVD process, generally, methane (CH_4) is used as a carbon source, while NH_3 is adopted as the N source. Besides gas-phase precursors, liquid or solid organic molecules are also

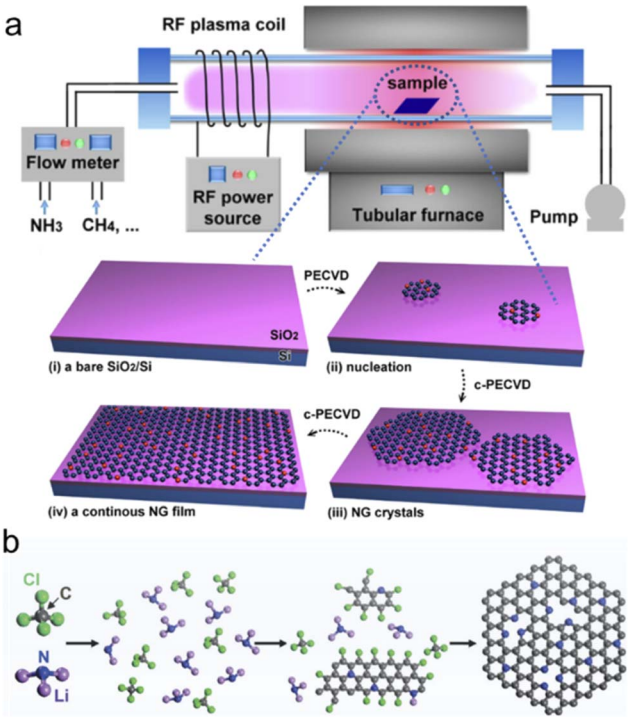

Fig. 4 Synthesis of NG by (a) the CVD method and (b) the WRC reaction. (a–c) Reprinted with permission from ref. 65 and 72, 2011 and 2015 copyright© American Chemical Society, respectively.

employed as precursors, such as pyridine,[66] acrylonitrile,[67] hexaphenylborazine[68] and pentachloropyridine.[69] The structure and quality of the resulting NG films were correlated with the functional groups of the precursor molecules and gas phase composition. For example, amine functional groups in methylamine can lead to a direct growth of graphene even without additional H_2 in the gas phase, which indicates that the intermediate species (*e.g.*, amine radicals) in the gas phase can significantly enhance the growth kinetics of graphene.[70]

3.2.2 Solvothermal method. The Wurtz-type reductive coupling (WRC) reaction is also a bottom-up method for the preparation of high-quality graphene by a solvothermal reaction of tetrachloromethane (CCl_4) with metal potassium (K).[71] Deng *et al.* synthesized two types of NG by utilized CCl_4 or cyanuric chloride as the carbon source and lithium nitride as the nitrogen source in a stainless steel autoclave filled with N_2 gas at 250 ~ 350 °C for several hours (Fig. 4b).[72] The products were washed sequentially with 18 wt% HCl aqueous solution, water, and ethanol, followed by drying at 120 °C for 12 h. Pentachloropyridine was also employed as the C and N source to react with K in an autoclave.[73] Our group also used CCl_4 as the carbon source and an appropriate amount of pyrrole as the nitrogen source to react with metallic K at 200 °C for 6 h and finally obtained NG with a certain N content.[74,75] The doping level can be readily controlled by the amount of N-containing precursors for the synthesis.

Besides these two typical bottom-up methods, electrochemical bottom-up synthesis or bottom-up self-assembly was also developed to synthesize NG, strictly speaking, N-doped

graphene quantum dots or graphene nanoribbons.[76] Tian *et al.* used *o*-phenylenediamine as the reactant in pure water as the electrolyte and applied a constant voltage of 500 V between two high-purity Pt sheets for more than 1 hour at 25 °C at a stirring rate of 1000 rpm. The colorless solution gradually turned yellow indicating the formation of NG with a size from 2 to 6 nm.[77] Sinitskii and coworkers synthesized high-quality chevron-like N-doped graphene nanoribbons *via* Yamamoto coupling of molecular precursors containing nitrogen atoms followed by cyclodehydrogenation *via* the Scholl reaction.[78]

4. Electrocatalysis applications

4.1 Oxygen reduction reaction

The oxygen reduction reaction (ORR) is a critical reaction occurring at the cathode of fuel cells and metal-air batteries. Due to the sluggish reaction kinetics, precious Pt-based electrocatalysts are commonly used to boost the reaction, which usually accounts for almost half of the cost of fuel cells. To replace the commercial Pt-based electrocatalysts, many noble-metal-free materials have been developed, among which carbon-based materials are promising alternatives, especially N-doped carbon materials. As one of the N-doped carbon materials, NG not only holds the advantages of carbon materials (*e.g.*, good electrical conductivity), but also possesses the unique features of graphene (*e.g.*, high specific surface area and charge redistribution), which exhibits a highly promising prospect in the future.[26]

The ORR is a multi-step reaction proceeding through either a direct 4e pathway or a two-step 2e pathway, which highly depends on the activity of the electrocatalyst. In an acidic medium, the possible reaction pathways are expressed as eqn (1)–(3), while those in alkaline solution are expressed as eqn (4)–(6).[79]

In an acidic medium,

$$4e\ \text{pathway: } O_2 + 4H^+ + 4e^- \rightarrow 2H_2O \quad (1)$$

$$2e\ \text{pathway: } O_2 + 2H^+ + 2e^- \rightarrow H_2O_2 \quad (2)$$

$$H_2O_2 + 2H^+ + 2e^- \rightarrow H_2O \quad (3)$$

In an alkaline medium,

$$4e\ \text{pathway: } O_2 + 2H_2O + 4e^- \rightarrow 4OH^- \quad (4)$$

$$2e\ \text{pathway: } O_2 + H_2O + 2e^- \rightarrow HO_2^- + OH^- \quad (5)$$

$$HO_2^- + H_2O + 2e^- \rightarrow 3OH^- \quad (6)$$

A good selectivity of NG for the 4e reaction pathway is preferred in the application of fuel cells and metal-air batteries. For the reaction pathway in an alkaline medium, there are two

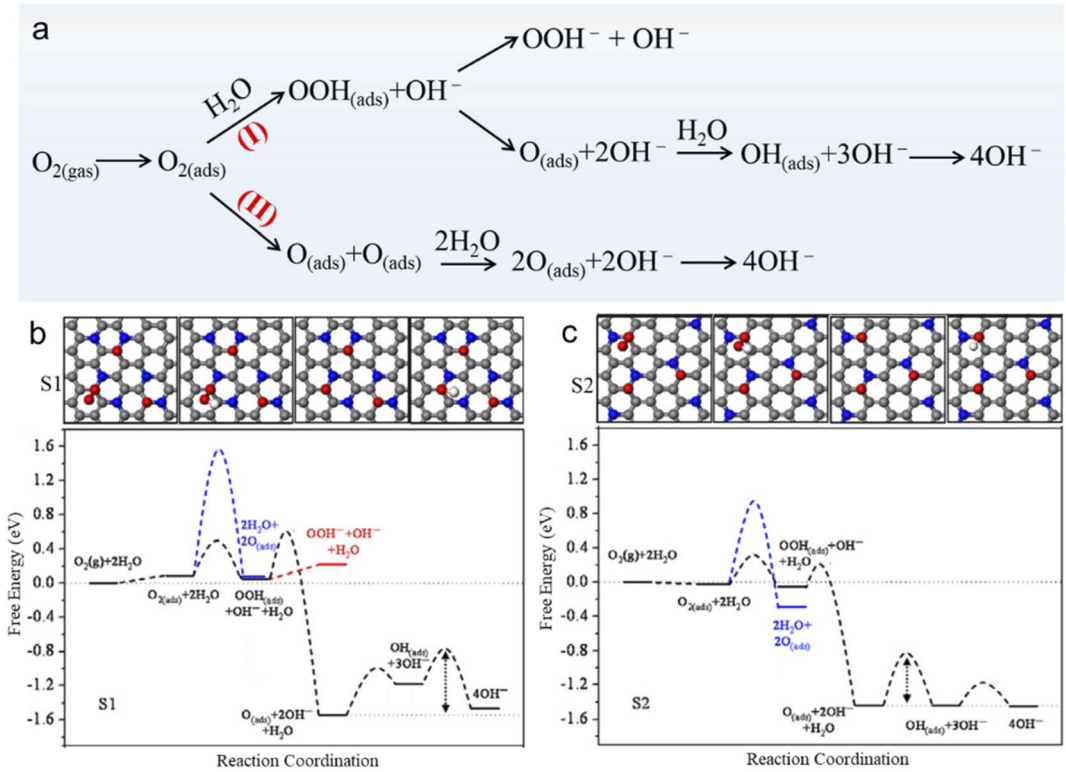

Fig. 5 (a) ORR pathways on NG in alkaline solution, where (I) presents an associative mechanism and (II) is a dissociative mechanism. (b) Free energy diagram for O_2 reduction on S_1 and S_2 under the conditions of 0.04 V and pH = 14. (c) Intermediate structures of the associative mechanism on S_1 and S_2. The gray, blue, red, and white spheres represent C, N, O, and H atoms, respectively. Reprinted with permission from ref. 80, Copyright©2012 Elsevier Inc.

different mechanisms, *i.e.*, associative mechanism and dissociative mechanism, as shown in Fig. 5a.[80] A density functional theory (DFT) study reveals that the associative mechanism (black line) on two surfaces (S1 and S2) of NG is more energetically favorable than the dissociative one (blue line), as shown in Fig. 5b and c. In S_1 and S_2, N atoms are separated by two C atoms and three C atoms, respectively, so S_1 possesses a more concentrated N distribution than S_2. The generation of OOH^- is represented by the red line. The results show that the rate-determining step (RDS) in the associative mechanism is the removal of $O_{(ads)}$ species from the active site. And the formation energy of $O_{(ads)}$ on S_1 is always lower (more exothermic) than that on S_2, which is attributed to the higher local concentration of N atoms on S_1 than that on S_2.

The real active sites in NG have been an attractive research topic due to contradictory opinions: carbon atoms adjacent to the N dopant, graphite-N or pyridine-N, or both. For example, Sidik and coworkers reported that substitutional N atoms from the graphite sheet edges are more active than those close to the edges.[81] Niwa *et al.* also found that catalysts with more graphite N exhibit a higher ORR activity than those with more pyridine N.[82] Huang *et al.* suggested that graphite N next to the zigzag edge enhances the O_2 adsorption and the subsequent ORR

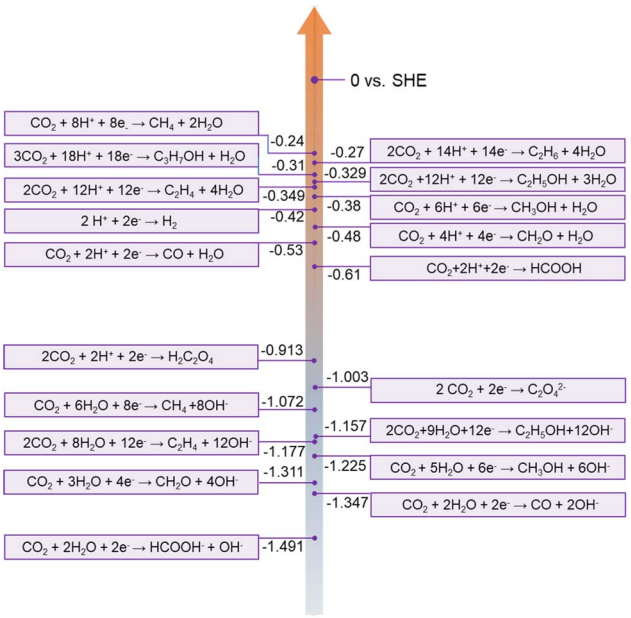

Fig. 7 CO_2RR at different standard potentials in aqueous solution at pH = 7.0, 1.0 atm, and 25°C. Reprinted with permission from ref. 26, copyright© 2019 The Royal Society of Chemistry.

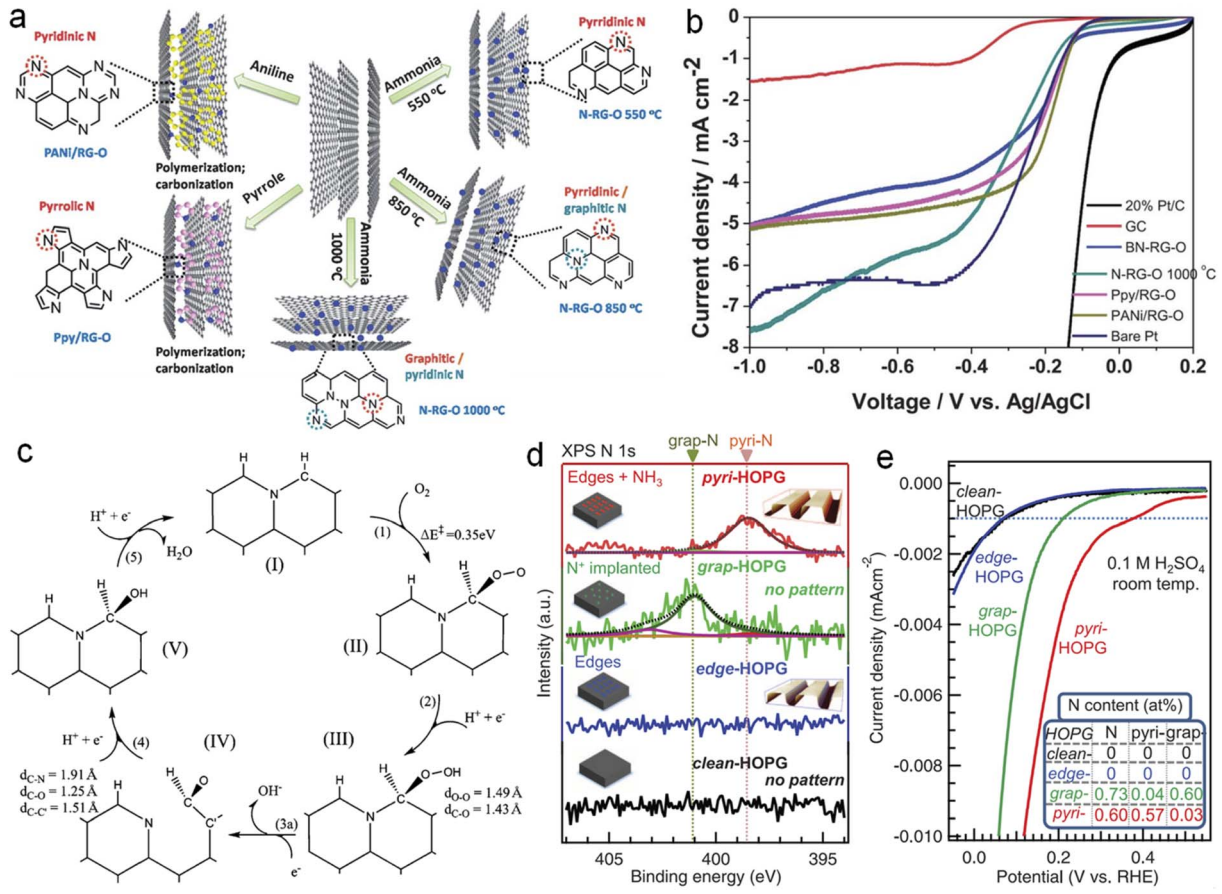

Fig. 6 (a) Scheme for synthesis and (b) LSV curves of NG with different N species, (c) a proposed ORR catalytic cycle for graphitic-N doped graphene, (d) N 1s XPS spectra of model catalysts and (e) corresponding ORR polarization curves. (a and b) and (c) reprinted with permission from ref. 83 and 84, copyright© 2013 and 2011 The Royal Society of Chemistry, respectively. (d and e) Reprinted with permission from ref. 85. copyright© 2016 AAAS.

process to two H_2O with a small activation barrier of about 5 kcal mol^{-1}, whereas the graphite N inside the graphene sheet does not contribute to ORR activity.[37] Lai *et al.* synthesized different NG samples as shown in Fig. 6a by using different N-containing precursors and found that the limiting diffusion current (j_L) and the onset potential (E_{onset}) are governed by graphitic-N and pyridinic-N, respectively (Fig. 6b).[83] Jung's group found that graphitic N in particular enables improved ORR activity and becomes pyridinic N (stage IV) in the next transfer reaction of electrons and protons *via* the ring-opening of a cyclic C–N bond as shown in step (3a) in Fig. 6c.[84] And the projected density of states (pDOS) and the orbital shape of N in stage (IV) are highly similar to those of typical pyridinic N. Recently, Guo *et al.* tactfully designed pyridinic N-dominated HOPG (pyri-HOPG) and graphitic N-dominated HOPG (grap-HOPG) as evidenced by Fig. 6d and proved that Lewis basic C atoms neighboring pyridinic N instead of pyridinic N themselves are active sites toward the ORR as illustrated by the polarization curves in Fig. 6e.[85]

Although there are unconsistent opinions on the function of different N species, there is no doubt that the introduction of N heteroatoms induces a positive charge density on an adjacent C atom, due to the high electronegativity of N.[22] The redistribution of electrons facilitates the adsorption and subsequent reduction process. Zhang *et al.* theoretically calculated the atomic charge density and spin density of pristine graphene and NG by constructing the models of $C_{46}H_{18}$ and $C_{45}NH_{18}$.[86] They pointed out that N-doping would promote the electrons to be easily excited from the valence band to the conduction band, because N doping introduces an unpaired electron and causes the localized distribution of molecule orbitals. Moreover, spin density is more important than atomic charge density in determining the catalytically active sites. Generally, carbon atoms with the highest spin density are the electrocatalytically active sites. These findings inspire the modulation of carbon-based materials toward a high-performance ORR, such as introducing other types of heteroatom or carbon defects to adjust the electronic structure or create more exposed active sites.

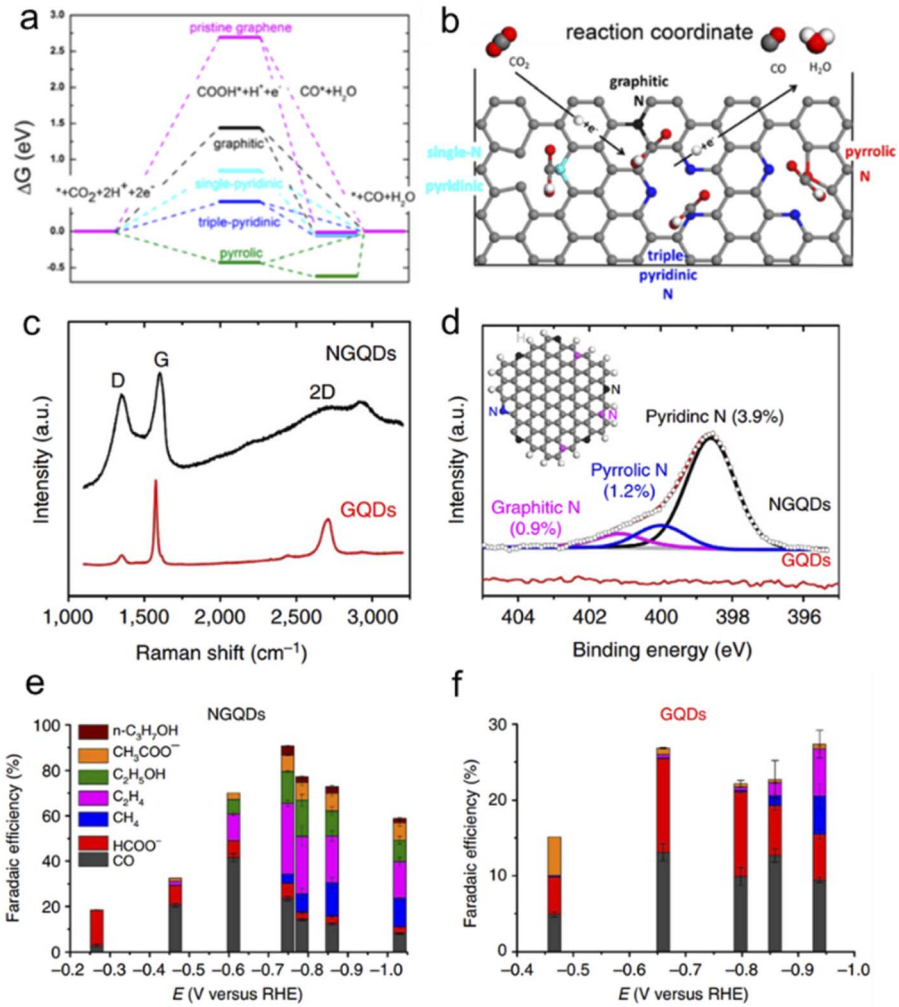

Fig. 8 (a) Free energy diagram of electrochemical reduction of CO_2 to CO on NG and (b) schematic of N configuration and the CO_2 reduction pathway. (c) Raman spectrum of NGQDs as compared with that of pristine GQDs. (d) High-resolution N 1s spectrum for NGQDs, deconvoluted into three sub-peaks representing pyridinic, pyrrolic and graphitic N. The inset shows a scheme of NGQDs with zigzag edges and pyridinic (black), pyrrolic (blue) and graphitic (pink) N. (a and b) Reprinted with permission from ref. 92, copyright©2016 American Chemical Society.

4.2 CO_2 reduction reaction

Carbon neutrality has become a global goal, which is desired to achieve net-zero carbon dioxide (CO_2) emissions. Enormous efforts have also been made by worldwide researchers. The electrochemical CO_2RR is an effective approach to realize the conversion from CO_2 to value-added chemical products.[87] The CO_2 molecule consisting of two linear C=O bonds is thermodynamically stable and chemically inert, due to a bond dissociation energy of 750 kJ mol^{-1}, which is difficult to reduce.[88] Moreover, the CO_2RR becomes more challenging in an aqueous electrolyte, due to the competition of the hydrogen evolution reaction (HER) and the diversity of products. Generally, the CO_2RR involves 2 to 18 electrons depending on different pathways as shown in Fig. 7. Therefore, electrocatalysts with high selectivity and activity toward CO_2 are necessary.

Inspired by the achievements of NG toward the ORR, researchers have also studied the electrocatalytic performance and mechanism of N-doped carbon materials. For example, Kumar *et al.* reported that N-doped carbon nanofibers (N-CNFs) are able to reduce CO_2 to CO at a low overpotential of 0.17 V *vs.* SHE and exhibit exceptionally high current densities (~13 times higher than that of bulk Ag) and a high FE of 98% for CO formation at −0.573 V *vs.* SHE.[89] They proposed that the naturally oxidized carbon atoms with positive charge and later reduced C atoms adjacent to pyridinic-N in N-CNFs were responsible for the CO_2RR. Sharma *et al.* also reported that the presence of graphitic and pyridinic nitrogen significantly decreases the overpotential and increases the selectivity towards the formation of CO.[90]

Ajayan's group conducted a series of experiments to improve the performance of the CO_2RR. Firstly, they synthesized N-doped CNTs (N-CNTs) and obtained good CO_2RR performance with an overpotential of −0.18 V and a selectivity of 80%.[91] They thought that pyridinic N as a catalytic site possesses a low free energy for CO_2 activation and a high barrier for hydrogen evolution. Moreover, by assembling NG to 3D foam, they improved the faradaic efficiency for CO production to ~85% at a lower overpotential

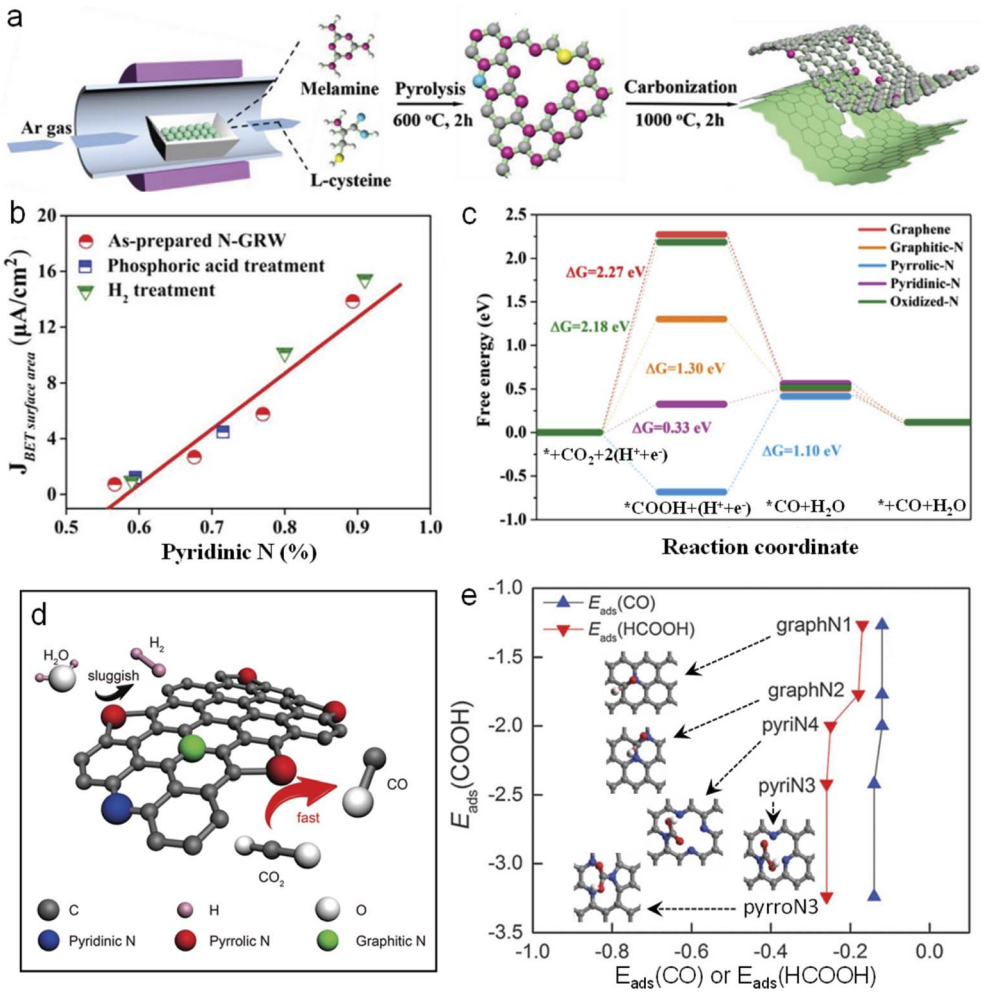

Fig. 9 (a) Schematic diagram of the synthesis processes of N-GRW. (b) The relationship between the CO partial current density and the pyridinic N content in various N-GRW catalysts at 0.5 V *versus* RHE. (c) Free energy diagram of the CO_2RR on various N-GRW catalysts. (d) Schematic illustration of the electrochemical CO_2RR of N-doped carbon with abundant pyrrolic N and passivation for the HER. (a–c) and (d) Reprinted with permission from ref. 95 and 96, copyright© 2018 and 2017 WILEY-VCH, respectively. (e) Reprinted with permission from ref. 97, copyright © The Royal Society of Chemistry.

(−0.47 V) and stability for at least 5 h.[92] DFT calculations show that the uphill free energy barrier comes from the first proton-coupled electron transfer step to form COOH* and drops dramatically upon introducing dangling N bonds (Fig. 8a & b). Triple-pyridinic N maximally lowers the barrier of the COOH* adsorption step followed by single pyridinic and graphitic N. Although COOH* adsorbing on pyrrolic N site is exergonic, the release of chemisorbed CO from pyrrolic-N is endothermic with an energy barrier of ∼0.6 eV (Fig. 8a). To increase the density of pyridinic N, they prepared nanometer-size N-doped graphene quantum dots (NGQDs) as shown in Fig. 8c and d. The NGQDs show a high total faradaic efficiency of up to 90% for the CO_2RR, and the selectivity for ethylene (C_2H_4) and ethanol (EtOH and C_2H_5OH) conversions reaches 45% (Fig. 8e and f).[93] The C2 and C3 product distribution and production rate for the CO_2RR are comparable to those of Cu-based electrocatalysts. Theoretical calculations reveal that NGQDs can electrochemically convert CO_2 to various hydrocarbons and oxygenates, including CH_4, C_2H_4, and C_2H_5OH, which begin with effective reduction of CO_2 to CO, promoted by enhanced binding between *COOH and NGQDs.[94] It is found that water-assisted H shuttling significantly reduces the barrier for the generation of $*CH_2$, the precursor for CH_4, and the formation of C2 products critically depends on the coupling of C1 products, *i.e.*,$*CH_2$ and CO.

Recently, Liu's group synthesized a 3D N-doped graphene nanoribbon network (N-GRW) by using melamine and L-cysteine as reactants (Fig. 9a) and investigated its electrocatalytic activity toward the CO_2RR.[95] They found that only the current density of CO formation exhibits a linear regression with the concentration of pyridinic N as shown in Fig. 9b. To further verify the role of pyridinic N, they tuned the content of pyridinic N in N-GRW by a post-hydrogen treatment or phosphoric acid treatment. The results demonstrate that the activity of the CO_2RR changes according to the content of pyridinic N. DFT calculations also reveal that the bonding between COOH and pyridinic N is in a suitable state (neither too strong nor too weak) as shown in Fig. 9c, which is conducive to the transformation of CO_2 to *COOH and further to *CO. In contrast, Zheng's group selectively etched graphitic N and pyridinic N by using water steam and retained pyrrolic N in the N-doped carbon catalyst as shown in Fig. 9d.[96] This steam-etched N-doped carbon with abundant pyrrolic N shows excellent CO_2RR performance but low HER activity, exhibiting a high CO_2RR selectivity (≈88%) toward the formation of CO under −0.5 V *versus* RHE. By virtue of DFT calculations, Liu found that pyrrolic N-doped graphene is the most efficient with an overpotential of 0.24 V among four types of N species (Fig. 9e).[97] Moreover, the pyrrolic N reduces the free energy barrier of the RDS to form the key intermediate COOH and exclusively leads to HCOOH as the product.

5. Conclusion and outlook

In summary, we review the advances of NG with respect to fundamental properties, synthesis and electrocatalytic applications toward the ORR and CO_2RR. As a promising alternative to noble meal catalysts, NG has exhibited promising potential to use in these two energy-conversion reactions. Because of the ideal 2D structure, it provides a good platform for exploring the underlying electrocatalytic mechanism behind the superior performance by both theoretical calculations and experiments. But it is still challenging to design and synthesize targeted NG with good selectivity and activity for the ORR or CO_2RR. Developing advanced synthetic methods is an important precondition to guarantee a precise synthesis of NG with specific N species. In this regard, a bottom-up strategy holds a unique advantage, especially by coupling reaction between organic molecules with specific N species.[98,99]

The complexity of N species in NG induces difficulty in uncovering the underlying electrocatalytic mechanism. Solid evidence on the electrocatalytic process and mechanism will be well revealed with the development of computational power and characterization techniques,[100] such as *in situ*/operando Fourier Transform Infrared Spectroscopy (FTIR) and *in situ*/operando X-ray absorption spectroscopy (XAS).[101,102] It is even necessary to establish an "*in situ* probing map" consisting of complementary aspects of electrocatalysts to track the dynamic process and identify the real active species systematically.[102] Theoretically, machine learning is a powerful strategy to almost exhaustively screen NG with various N species and predict the desirable NG electrocatalyst.[103–106] The combination of high-throughput screening of big data with purposeful experiments would open a new avenue for the development of NG used as an electrocatalyst.

Besides being a good candidate for electrocatalysts, NG also displays structural advantages to anchor single metal atoms due to the intrinsic defects of NG, thus forming high-performance single-atomic catalysts (SACs).[107–109] For example, Sun's group fabricated single platinum atoms on NG nanosheets for hydrogen evolution by using the atomic layer deposition (ALD) technique, resulting in the utilization of nearly all the Pt atoms.[110] Fei *et al.* synthesized a series of atomic 3d metals embedded in N-doped holey graphene and investigated the electrocatalytic performance toward the oxygen evolution reaction.[111] The synthesis of SACs by using NG or N-doped carbon materials has become an important strategy.[112] The flourishing of SACs would move forward the understanding of the catalytic mechanism and development of low-cost catalysts with high performance toward various catalytic reactions not only limited to the ORR and CO_2RR.

Conflicts of interest

There are no conflicts to declare.

Acknowledgements

The authors are grateful for financial support from the National Natural Science Foundation of China (52172058).

References

1 J. Fu, Z. P. Cano, M. G. Park, A. Yu, M. Fowler and Z. Chen, *Adv. Mater.*, 2017, **29**, 1604685.
2 S. Wang and S. P. Jiang, *Natl. Sci. Rev.*, 2017, **4**, 163–166.

3 R. Ma, G. Lin, Y. Zhou, Q. Liu, T. Zhang, G. Shan, M. Yang and J. Wang, *npj Comput. Mater.*, 2019, **5**, 78.
4 L. An, Y. Hu, J. Li, J. Zhu, M. Sun, B. Huang, P. Xi and C.-H. Yan, *Adv. Mater.*, 2022, **34**, 2202874.
5 G. Wang, J. Chen, Y. Ding, P. Cai, L. Yi, Y. Li, C. Tu, Y. Hou, Z. Wen and L. Dai, *Chem. Soc. Rev.*, 2021, **50**, 4993–5061.
6 J. Wu, Y. Huang, W. Ye and Y. Li, *Adv. Sci.*, 2017, **4**, 1700194.
7 J. Yin, Z. Yin, J. Jin, M. Sun, B. Huang, H. Lin, Z. Ma, M. Muzzio, M. Shen, C. Yu, H. Zhang, Y. Peng, P. Xi, C.-H. Yan and S. Sun, *J. Am. Chem. Soc.*, 2021, **143**, 15335–15343.
8 Y. P. Zhu, C. Guo, Y. Zheng and S.-Z. Qiao, *Acc. Chem. Res.*, 2017, **50**, 915–923.
9 H. Jing, P. Zhu, X. Zheng, Z. Zhang, D. Wang and Y. Li, *Advanced Powder Materials*, 2022, **1**, 100013.
10 K. S. Novoselov, V. I. Fal′ko, L. Colombo, P. R. Gellert, M. G. Schwab and K. Kim, *Nature*, 2012, **490**, 192–200.
11 H. Tao, Y. Gao, N. Talreja, F. Guo, J. Texter, C. Yan and Z. Sun, *J. Mater. Chem. A*, 2017, **5**, 7257–7284.
12 X. Zhang, A. Chen, L. Chen and Z. Zhou, *Adv. Energy Mater.*, 2022, **12**, 2003841.
13 X. Zhan, C. Si, J. Zhou and Z. Sun, *Nanoscale Horiz.*, 2020, **5**, 235–258.
14 R. Qin, G. Shan, M. Hu and W. Huang, *Mater. Today Phys.*, 2021, **21**, 100527.
15 H. Li, J. Wu, Z. Yin and H. Zhang, *Acc. Chem. Res.*, 2014, **47**, 1067–1075.
16 Y. Xu, B. Li, S. Zheng, P. Wu, J. Zhan, H. Xue, Q. Xu and H. Pang, *J. Mater. Chem. A*, 2018, **6**, 22070–22076.
17 Y. Yan, J. Gong, J. Chen, Z. Zeng, W. Huang, K. Pu, J. Liu and P. Chen, *Adv. Mater.*, 2019, **31**, 1808283.
18 S. Dutta and S. K. Pati, *J. Mater. Chem.*, 2010, **20**, 8207–8223.
19 J. Bai, X. Zhong, S. Jiang, Y. Huang and X. Duan, *Nat. Nanotechnol.*, 2010, **5**, 190–194.
20 Y. Cao, V. Fatemi, S. Fang, K. Watanabe, T. Taniguchi, E. Kaxiras and P. Jarillo-Herrero, *Nature*, 2018, **556**, 43–50.
21 R. Ma, Y. Zhou, H. Bi, M. Yang, J. Wang, Q. Liu and F. Huang, *Prog. Mater. Sci.*, 2020, **113**, 100665.
22 Z. Zhao, M. Li, L. Zhang, L. Dai and Z. Xia, *Adv. Mater.*, 2015, **27**, 6834–6840.
23 M. Inagaki, M. Toyoda, Y. Soneda and T. Morishita, *Carbon*, 2018, **132**, 104–140.
24 K. Gong, F. Du, Z. Xia, M. Durstock and L. Dai, *Science*, 2009, **323**, 760–764.
25 Y. Shao, Z. Jiang, Q. Zhang and J. Guan, *ChemSusChem*, 2019, **12**, 2133–2146.
26 L. Qu, Y. Liu, J.-B. Baek and L. Dai, *ACS Nano*, 2010, **4**, 1321–1326.
27 H. Cui, Y. Guo, L. Guo, L. Wang, Z. Zhou and Z. Peng, *J. Mater. Chem. A*, 2018, **6**, 18782–18793.
28 X. Duan, J. Xu, Z. Wei, J. Ma, S. Guo, S. Wang, H. Liu and S. Dou, *Adv. Mater.*, 2017, **29**, 1701784.
29 D. M. Fernandes, A. F. Peixoto and C. Freire, *Dalton Trans.*, 2019, **48**, 13508–13528.
30 S. Casolo, R. Martinazzo and G. F. Tantardini, *J. Phys. Chem. C*, 2011, **115**, 3250–3256.
31 L. Zhao, R. He, K. T. Rim, T. Schiros, K. S. Kim, H. Zhou, C. Gutiérrez, S. P. Chockalingam, C. J. Arguello, L. Pálová, D. Nordlund, M. S. Hybertsen, D. R. Reichman, T. F. Heinz, P. Kim, A. Pinczuk, G. W. Flynn and A. N. Pasupathy, *Science*, 2011, **333**, 999–1003.
32 T. Kondo, S. Casolo, T. Suzuki, T. Shikano, M. Sakurai, Y. Harada, M. Saito, M. Oshima, M. I. Trioni, G. F. Tantardini and J. Nakamura, *Phys. Rev. B*, 2012, **86**, 035436.
33 M. Zhang and L. Dai, *Nano Energy*, 2012, **1**, 514–517.
34 A. Lherbier, A. R. Botello-Méndez and J.-C. Charlier, *Nano Lett.*, 2013, **13**, 1446–1450.
35 R. Lv, Q. Li, A. R. Botello-Méndez, T. Hayashi, B. Wang, A. Berkdemir, Q. Hao, A. L. Elías, R. Cruz-Silva, H. R. Gutiérrez, Y. A. Kim, H. Muramatsu, J. Zhu, M. Endo, H. Terrones, J.-C. Charlier, M. Pan and M. Terrones, *Sci. Rep.*, 2012, **2**, 586.
36 X. Wang, Z. Hou, T. Ikeda, S.-F. Huang, K. Terakura, M. Boero, M. Oshima, M.-a. Kakimoto and S. Miyata, *Phys. Rev. B*, 2011, **84**, 245434.
37 S.-F. Huang, K. Terakura, T. Ozaki, T. Ikeda, M. Boero, M. Oshima, J.-I. Ozaki and S. Miyata, *Phys. Rev. B*, 2009, **80**, 235410.
38 X. Wang, Z. Hou, T. Ikeda, M. Oshima, M.-A. Kakimoto and K. Terakura, *J. Phys. Chem. A*, 2013, **117**, 579–589.
39 Z. Li, R. Ma, Q. Ju, Q. Liu, L. Liu, Y. Zhu, M. Yang and J. Wang, *Innovation*, 2022, **3**, 100268.
40 J. Zhong, J.-J. Deng, B.-H. Mao, T. Xie, X.-H. Sun, Z.-G. Mou, C.-H. Hong, P. Yang and S.-D. Wang, *Carbon*, 2012, **50**, 335–338.
41 R. S. Edwards and K. S. Coleman, *Nanoscale*, 2013, **5**, 38–51.
42 J. M. Tour, *Chem. Mater.*, 2014, **26**, 163–171.
43 X. Li, H. Wang, J. T. Robinson, H. Sanchez, G. Diankov and H. Dai, *J. Am. Chem. Soc.*, 2009, **131**, 15939–15944.
44 G. Lemes, D. Sebastián, E. Pastor and M. J. Lázaro, *J. Power Sources*, 2019, **438**, 227036.
45 L. Sun, L. Wang, C. Tian, T. Tan, Y. Xie, K. Shi, M. Li and H. Fu, *RSC Adv.*, 2012, **2**, 4498–4506.
46 D. Voiry, J. Yang, J. Kupferberg, R. Fullon, C. Lee, H. Y. Jeong, H. S. Shin and M. Chhowalla, *Science*, 2016, **353**, 1413–1416.
47 S. P. Economopoulos, G. Rotas, Y. Miyata, H. Shinohara and N. Tagmatarchis, *ACS Nano*, 2010, **4**, 7499–7507.
48 R. Jakhar, J. E. Yap and R. Joshi, *Carbon*, 2020, **170**, 277–293.
49 J. Sun, W. Wang and Q. Yue, *Materials*, 2016, **9**, 231.
50 C. Wang, X. Han, P. Xu, X. Zhang, Y. Du, S. Hu, J. Wang and X. Wang, *Appl. Phys. Lett.*, 2011, **98**, 072906.
51 Y. Xin, J. G. Liu, X. Jie, W. Liu, F. Liu, Y. Yin, J. Gu and Z. Zou, *Electrochim. Acta*, 2012, **60**, 354–358.
52 Y.-H. Lee, K.-H. Chang and C.-C. Hu, *J. Power Sources*, 2013, **227**, 300–308.
53 A. Dey, A. Chroneos, N. S. J. Braithwaite, R. P. Gandhiraman and S. Krishnamurthy, *Appl. Phys. Rev.*, 2016, **3**, 021301.
54 I. Bertóti, M. Mohai and K. László, *Carbon*, 2015, **84**, 185–196.
55 Y. Wang, Y. Shao, D. W. Matson, J. Li and Y. Lin, *ACS Nano*, 2010, **4**, 1790–1798.

56 H. M. Jeong, J. W. Lee, W. H. Shin, Y. J. Choi, H. J. Shin, J. K. Kang and J. W. Choi, *Nano Lett.*, 2011, **11**, 2472–2477.
57 S. Sakulsermsuk, P. Singjai and C. Chaiwong, *Diamond Relat. Mater.*, 2016, **70**, 211–218.
58 K. S. Subrahmanyam, L. S. Panchakarla, A. Govindaraj and C. N. R. Rao, *J. Phys. Chem. C*, 2009, **113**, 4257–4259.
59 N. Li, Z. Wang, K. Zhao, Z. Shi, Z. Gu and S. Xu, *Carbon*, 2010, **48**, 255–259.
60 W. Qian, X. Cui, R. Hao, Y. Hou and Z. Zhang, *ACS Appl. Mater. Interfaces*, 2011, **3**, 2259–2264.
61 I. Choi, H. Y. Jeong, D. Y. Jung, M. Byun, C.-G. Choi, B. H. Hong, S.-Y. Choi and K. J. Lee, *ACS Nano*, 2014, **8**, 7671–7677.
62 Y. Zhang, B. Cao, B. Zhang, X. Qi and C. Pan, *Thin Solid Films*, 2012, **520**, 6850–6855.
63 Y. Zhang, L. Zhang and C. Zhou, *Acc. Chem. Res.*, 2013, **46**, 2329–2339.
64 A. Cabrero-Vilatela, R. S. Weatherup, P. Braeuninger-Weimer, S. Caneva and S. Hofmann, *Nanoscale*, 2016, **8**, 2149–2158.
65 D. Wei, L. Peng, M. Li, H. Mao, T. Niu, C. Han, W. Chen and A. T. S. Wee, *ACS Nano*, 2015, **9**, 164–171.
66 Y. Xue, B. Wu, L. Jiang, Y. Guo, L. Huang, J. Chen, J. Tan, D. Geng, B. Luo, W. Hu, G. Yu and Y. Liu, *J. Am. Chem. Soc.*, 2012, **134**, 11060–11063.
67 G. Imamura and K. Saiki, *J. Phys. Chem. C*, 2011, **115**, 10000–10005.
68 G. Imamura, C. W. Chang, Y. Nabae, M.-a. Kakimoto, S. Miyata and K. Saiki, *J. Phys. Chem. C*, 2012, **116**, 16305–16310.
69 J. Zhang, J. Li, Z. Wang, X. Wang, W. Feng, W. Zheng, W. Cao and P. Hu, *Chem. Mater.*, 2014, **26**, 2460–2466.
70 Y. Ito, C. Christodoulou, M. V. Nardi, N. Koch, H. Sachdev and K. Müllen, *ACS Nano*, 2014, **8**, 3337–3346.
71 X. Lü, J. Wu, T. Lin, D. Wan, F. Huang, X. Xie and M. Jiang, *J. Mater. Chem.*, 2011, **21**, 10685–10689.
72 D. Deng, X. Pan, L. Yu, Y. Cui, Y. Jiang, J. Qi, W.-X. Li, Q. Fu, X. Ma, Q. Xue, G. Sun and X. Bao, *Chem. Mater.*, 2011, **23**, 1188–1193.
73 D. Geng, Y. Hu, Y. Li, R. Li and X. Sun, *Electrochem. Commun.*, 2012, **22**, 65–68.
74 R. Ma, X. Ren, B. Y. Xia, Y. Zhou, C. Sun, Q. Liu, J. Liu and J. Wang, *Nano Res.*, 2016, **9**, 808–819.
75 R. Ma, Y. Zhou, P. Li, Y. Chen, J. Wang and Q. Liu, *Electrochim. Acta*, 2016, **216**, 347–354.
76 C. Bronner, S. Stremlau, M. Gille, F. Brausse, A. Haase, S. Hecht and P. Tegeder, *Angew. Chem., Int. Ed.*, 2013, **52**, 4422–4425.
77 L. Tian, S. Yang, Y. Yang, J. Li, Y. Deng, S. Tian, P. He, G. Ding, X. Xie and Z. Wang, *RSC Adv.*, 2016, **6**, 82648–82653.
78 T. H. Vo, M. Shekhirev, D. A. Kunkel, F. Orange, M. J. F. Guinel, A. Enders and A. Sinitskii, *Chem. Commun.*, 2014, **50**, 4172–4174.
79 Y. Zheng, Y. Jiao, M. Jaroniec, Y. Jin and S. Z. Qiao, *Small*, 2012, **8**, 3550–3566.
80 L. Yu, X. Pan, X. Cao, P. Hu and X. Bao, *J. Catal.*, 2011, **282**, 183–190.
81 R. A. Sidik, A. B. Anderson, N. P. Subramanian, S. P. Kumaraguru and B. N. Popov, *J. Phys. Chem. B*, 2006, **110**, 1787–1793.
82 H. Niwa, K. Horiba, Y. Harada, M. Oshima, T. Ikeda, K. Terakura, J.-i. Ozaki and S. Miyata, *J. Power Sources*, 2009, **187**, 93–97.
83 L. Lai, J. R. Potts, D. Zhan, L. Wang, C. K. Poh, C. Tang, H. Gong, Z. Shen, J. Lin and R. S. Ruoff, *Energy Environ. Sci.*, 2012, **5**, 7936–7942.
84 H. Kim, K. Lee, S. I. Woo and Y. Jung, *Phys. Chem. Chem. Phys.*, 2011, **13**, 17505–17510.
85 D. Guo, R. Shibuya, C. Akiba, S. Saji, T. Kondo and J. Nakamura, *Science*, 2016, **351**, 361–365.
86 L. Zhang and Z. Xia, *J. Phys. Chem. C*, 2011, **115**, 11170–11176.
87 Z. Sun, T. Ma, H. Tao, Q. Fan and B. Han, *Chem*, 2017, **3**, 560–587.
88 Q. Lu and F. Jiao, *Nano Energy*, 2016, **29**, 439–456.
89 B. Kumar, M. Asadi, D. Pisasale, S. Sinha-Ray, B. A. Rosen, R. Haasch, J. Abiade, A. L. Yarin and A. Salehi-Khojin, *Nat. Commun.*, 2013, **4**, 2819.
90 P. P. Sharma, J. Wu, R. M. Yadav, M. Liu, C. J. Wright, C. S. Tiwary, B. I. Yakobson, J. Lou, P. M. Ajayan and X.-D. Zhou, *Angew. Chem., Int. Ed.*, 2015, **54**, 13701–13705.
91 J. Wu, R. M. Yadav, M. Liu, P. P. Sharma, C. S. Tiwary, L. Ma, X. Zou, X.-D. Zhou, B. I. Yakobson, J. Lou and P. M. Ajayan, *ACS Nano*, 2015, **9**, 5364–5371.
92 J. Wu, M. Liu, P. P. Sharma, R. M. Yadav, L. Ma, Y. Yang, X. Zou, X.-D. Zhou, R. Vajtai, B. I. Yakobson, J. Lou and P. M. Ajayan, *Nano Lett.*, 2016, **16**, 466–470.
93 J. Wu, S. Ma, J. Sun, J. I. Gold, C. Tiwary, B. Kim, L. Zhu, N. Chopra, I. N. Odeh, R. Vajtai, A. Z. Yu, R. Luo, J. Lou, G. Ding, P. J. A. Kenis and P. M. Ajayan, *Nat. Commun.*, 2016, **7**, 13869.
94 X. Zou, M. Liu, J. Wu, P. M. Ajayan, J. Li, B. Liu and B. I. Yakobson, *ACS Catal.*, 2017, **7**, 6245–6250.
95 S. Liu, H. Yang, X. Huang, L. Liu, W. Cai, J. Gao, X. Li, T. Zhang, Y. Huang and B. Liu, *Adv. Funct. Mater.*, 2018, **28**, 1800499.
96 X. Cui, Z. Pan, L. Zhang, H. Peng and G. Zheng, *Adv. Energy Mater.*, 2017, **7**, 1701456.
97 Y. Liu, J. Zhao and Q. Cai, *Phys. Chem. Chem. Phys.*, 2016, **18**, 5491–5498.
98 A. Jolly, D. Miao, M. Daigle and J.-F. Morin, *Angew. Chem., Int. Ed.*, 2020, **59**, 4624–4633.
99 J. Cai, P. Ruffieux, R. Jaafar, M. Bieri, T. Braun, S. Blankenburg, M. Muoth, A. P. Seitsonen, M. Saleh, X. Feng, K. Müllen and R. Fasel, *Nature*, 2010, **466**, 470–473.
100 X. Li, S. Wang, L. Li, Y. Sun and Y. Xie, *J. Am. Chem. Soc.*, 2020, **142**, 9567–9581.
101 J. Timoshenko and B. Roldan Cuenya, *Chem. Rev.*, 2021, **121**, 882–961.
102 Y. Zhu, J. Wang, H. Chu, Y.-C. Chu and H. M. Chen, *ACS Energy Lett.*, 2020, **5**, 1281–1291.

103 N. Zhang, B. Yang, K. Liu, H. Li, G. Chen, X. Qiu, W. Li, J. Hu, J. Fu, Y. Jiang, M. Liu and J. Ye, *Small Methods*, 2021, **5**, 2100987.
104 J. Liu, W. Luo, L. Wang, J. Zhang, X.-Z. Fu and J.-L. Luo, *Adv. Funct. Mater.*, 2022, **32**, 2110748.
105 S. Xu and E. A. Carter, *Chem. Rev.*, 2019, **119**, 6631–6669.
106 X. Yuan, L. Li, Z. Shi, H. Liang, S. Li and Z. Qiao, *Advanced Powder Materials*, 2022, **1**, 100026.
107 L. Zhang, Y. Ren, W. Liu, A. Wang and T. Zhang, *Natl. Sci. Rev.*, 2018, **5**, 653–672.
108 T. Zheng, K. Jiang, N. Ta, Y. Hu, J. Zeng, J. Liu and H. Wang, *Joule*, 2019, **3**, 265–278.
109 L. Yu, F. Li, J. Zhao and Z. Chen, *Advanced Powder Materials*, 2022, **1**, 100031.
110 N. Cheng, S. Stambula, D. Wang, M. N. Banis, J. Liu, A. Riese, B. Xiao, R. Li, T.-K. Sham, L.-M. Liu, G. A. Botton and X. Sun, *Nat. Commun.*, 2016, **7**, 13638.
111 H. Fei, J. Dong, Y. Feng, C. S. Allen, C. Wan, B. Volosskiy, M. Li, Z. Zhao, Y. Wang, H. Sun, P. An, W. Chen, Z. Guo, C. Lee, D. Chen, I. Shakir, M. Liu, T. Hu, Y. Li, A. I. Kirkland, X. Duan and Y. Huang, *Nat. Catal.*, 2018, **1**, 63–72.
112 J. Ma, X. Li, Y. Li, G. Jiao, H. Su, D. Xiao, S. Zhai and R. Sun, *Advanced Powder Materials*, 2022, **1**, 100058.